Nonadiabatic Dynamics of Hydrogen Tunneling with Nuclear-Electronic Orbital Multistate Density Functional Theory

Qi Yu[1], Saswata Roy[1,2], and Sharon Hammes-Schiffer[1*]

[1]Department of Chemistry, Yale University,
New Haven, Connecticut 06520 USA
[2]Current address: Department of Physics, Rutgers University,
101 Warren St, Newark, New Jersey, 07102 USA

[*]Corresponding author email: sharon.hammes-schiffer@yale.edu

Abstract

Proton transfer reactions play a critical role in many chemical and biological processes. The development of computationally efficient approaches to describe the quantum dynamics of proton transfer, which often involves hydrogen tunneling, is challenging. Herein, the nuclear-electronic orbital multistate density functional theory (NEO-MSDFT) method is combined with both Ehrenfest and surface hopping nonadiabatic dynamics methods to describe hydrogen tunneling. The NEO-MSDFT method treats the transferring hydrogen nucleus quantum mechanically on the same level as the electrons and incorporates both static and dynamical correlation by mixing localized NEO-DFT solutions with a nonorthogonal configuration interaction scheme. The other nuclei are propagated on the NEO-MSDFT vibronic surfaces during the Ehrenfest or surface hopping dynamics. These methods are applied to proton transfer in malonaldehyde as a prototypical hydrogen tunneling system. The inclusion of vibronically nonadiabatic effects is found to significantly impact the proton transfer time and tunneling dynamics. This approach is applicable to a wide range of other proton transfer reactions.

1. Introduction

Nuclear quantum effects such as hydrogen tunneling are important throughout chemistry and biology,[1-4] as exemplified by photosynthesis[5-6] and DNA synthesis.[7] The development of computational methods for describing hydrogen tunneling dynamics in chemical systems is challenging. The nuclear-electronic orbital (NEO) approach has become an accurate and efficient method to incorporate nuclear quantum effects in geometry optimizations, reaction paths, vibrational spectra, and dynamics of molecular systems.[8-16] This method treats electrons and specified nuclei, typically protons, quantum mechanically on the same level. In this case, the Born-Oppenheimer separation is not invoked between the electrons and quantum nuclei but is still invoked between the subsystem containing the electrons and quantum nuclei and the subsystem containing the other "classical" nuclei. By solving the mixed nuclear-electronic time-independent Schrödinger equation at each time step of a molecular dynamics trajectory, the classical nuclei can move on the vibronic surface that includes the nuclear delocalization and zero-point energy associated with the quantum nuclei.

Within the NEO framework, both wave function methods[8, 17-19] and density functional theory (DFT) methods[9-10, 20-21] have been developed. Recently, NEO-DFT based approaches have been successfully used for direct dynamics simulations describing various chemical reactions involving hydrogen transfer, where the transferring proton is treated quantum mechanically.[15, 22-23] For example, the NEO-DFT approach was employed to describe hydride transfer in the $C_4H_9^+$ molecular system.[15] Additionally, real-time NEO time-dependent DFT (NEO-TDDFT) and real-time NEO-TDDFT Ehrenfest dynamics were used to describe excited state intramolecular proton transfer in *o*-hydroxybenzaldehyde.[22-23]

In the conventional Born-Oppenheimer picture of hydrogen tunneling, the hydrogen typically moves on a double-well potential energy surface that becomes symmetric or nearly symmetric, with the hydrogen vibrational wavefunction delocalized over the two wells during tunneling.[24-26] In such cases, the NEO-DFT approach usually fails because the transferring proton density localizes near the hydrogen donor or acceptor, rather than delocalizing between them.[27-28] This non-physical localization is mainly attributed to insufficient inclusion of static and dynamical electron-proton correlation within the NEO-DFT method, which uses a single product of an electronic and nuclear determinant as the non-interacting reference system.

Inspired by the conventional electronic multistate density functional theory (MSDFT) method developed by Gao and coworkers,[29-32] we developed the NEO multistate density functional theory (NEO-MSDFT) method[33] to describe hydrogen transfer processes that involve a symmetric (or nearly symmetric) double-well potential energy surface in the conventional Born-Oppenheimer picture. The NEO-MSDFT approach incorporates both static and dynamical correlation by mixing two localized NEO-DFT solutions with a nonorthogonal configuration interaction scheme.[34-35] The ground and excited vibronic states obtained from the NEO-MSDFT approach can delocalize and become bilobal, which is essential for hydrogen tunneling systems. Moreover, the NEO-MSDFT method has been shown to accurately predict hydrogen tunneling splittings and proton densities for fixed classical nuclear configurations.[33] The NEO-MSDFT approach has the same computational cost scaling as the analogous conventional electronic DFT approach because the number of electronic basis functions is typically much greater than the number of protonic basis functions. Alternative multireference DFT approaches, as well as the associated challenges, are discussed elsewhere.[36-37]

Recently, we implemented the analytical gradients of the NEO-MSDFT ground and excited vibronic state energies with respect to the classical nuclear coordinates.[38] These gradients enable geometry optimizations to identify equilibrium structures and transition states, as well as the generation of minimum energy paths. We also explored the direct dynamics of the classical nuclei on the NEO-MSDFT adiabatic ground vibronic state surface and observed intramolecular proton transfer in malonaldehyde.[15] In the adiabatic approximation, however, the quantum proton responds instantaneously to motions of the classical nuclei. In this regime, within the conventional Born-Oppenheimer picture of a double-well potential energy surface, the proton always tunnels when the acceptor well becomes lower in energy than the donor well, regardless of the barrier height. As shown previously,[39] consideration of excited proton vibrational states is necessary to obtain a reasonable hydrogen tunneling probability. Similarly, contributions from the NEO-MSDFT excited vibronic state must be included to accurately describe hydrogen tunneling dynamics. Nonadiabatic dynamics approaches[40-41] such as Ehrenfest dynamics[42] or surface hopping[39, 43-44] are reasonable choices for describing hydrogen tunneling on the NEO-MSDFT vibronic surfaces.

Herein, we combine the NEO-MSDFT approach with both Ehrenfest dynamics and surface hopping dynamics. We derive the essential equations and provide the computational details for conducting these nonadiabatic dynamics simulations. The capability of the NEO-MSDFT approach for simulating adiabatic and nonadiabatic hydrogen tunneling dynamics is demonstrated by propagating representative trajectories for proton transfer in malonaldehyde, which is known to exhibit hydrogen tunneling.[24-26, 45-47] The objective of this work is to highlight the computational method rather than to comprehensively investigate the dynamics for this specific system. This paper is organized as follows. Section 2 provides a brief review of the NEO-MSDFT approach, as

well as the theoretical framework and computational details for combining this approach with adiabatic, Ehrenfest, and surface hopping dynamics. Section 3 presents the results from different types of dynamical simulations of proton transfer in malonaldehyde, along with an analysis of these results. Finally, Section 4 provides a summary of the current work and a discussion of future directions.

2. Methods and Computational Details

2.1. NEO-MSDFT method

Here we briefly introduce the NEO-MSDFT method for a single quantum proton and two vibronic states, but the extension to multiple quantum protons and more vibronic states is straightforward. More details on the formalism and implementation are provided in our previous papers.[33, 38] This treatment pertains to molecular systems with a double-well potential energy surface for proton transfer in the conventional Born-Oppenheimer picture. The NEO-DFT approach is employed first to generate two localized nuclear-electronic wave functions, $|\Psi_I\rangle = \Phi_I^e \Phi_I^p$ and $|\Psi_{II}\rangle = \Phi_{II}^e \Phi_{II}^p$, where each localized nuclear-electronic wave function is a product of Kohn-Sham electronic and protonic determinants, Φ^e and Φ^p, respectively. Due to the neglect of static correlation and the approximate electron-proton dynamical correlation energy treatment, each protonic wave function, Φ_I^p and Φ_{II}^p, obtained from the NEO-DFT approach is localized near the proton donor or acceptor. The NEO-MSDFT approach is used to construct the delocalized ground and excited vibronic states by solving a 2×2 matrix equation:

$$\mathbf{HD} = \mathbf{SDE} \tag{1}$$

Here **S** is the overlap matrix between the two localized states

$$\mathbf{S} = \begin{bmatrix} S_{\mathrm{I,I}} & S_{\mathrm{I,II}} \\ S_{\mathrm{II,I}} & S_{\mathrm{II,II}} \end{bmatrix} = \begin{bmatrix} 1 & \langle \Psi_{\mathrm{I}} | \Psi_{\mathrm{II}} \rangle \\ \langle \Psi_{\mathrm{II}} | \Psi_{\mathrm{I}} \rangle & 1 \end{bmatrix} \tag{2}$$

and **H** is the effective Hamiltonian given by

$$\mathbf{H} = \begin{bmatrix} H_{\mathrm{I,I}} & H_{\mathrm{I,II}} \\ H_{\mathrm{II,I}} & H_{\mathrm{II,II}} \end{bmatrix} \tag{3}$$

In Eq. (2), the off-diagonal matrix element of the overlap matrix, $S_{\mathrm{I,II}}$ or $S_{\mathrm{II,I}}$, is the overlap between the occupied electronic and protonic Kohn-Sham orbitals for states I and II. In terms of the electronic and protonic determinants, $S_{\mathrm{I,II}} = S_{\mathrm{II,I}} = \langle \Phi_{\mathrm{I}}^{\mathrm{e}} | \Phi_{\mathrm{II}}^{\mathrm{e}} \rangle \langle \Phi_{\mathrm{I}}^{\mathrm{p}} | \Phi_{\mathrm{II}}^{\mathrm{p}} \rangle$. In Eq. (3), the diagonal elements, $H_{\mathrm{I,I}}$ and $H_{\mathrm{II,II}}$, are the NEO-DFT energies of the two localized states such that $H_{\mathrm{I,I}} = E_{\mathrm{I}}^{\text{NEO-DFT}}$ and $H_{\mathrm{II,II}} = E_{\mathrm{II}}^{\text{NEO-DFT}}$. The off-diagonal element, $H_{\mathrm{I,II}}$, is approximated as

$$\begin{aligned} H_{\mathrm{I,II}} &= \langle \Psi_{\mathrm{I}} | \hat{H}_{\mathrm{NEO}} | \Psi_{\mathrm{II}} \rangle + \frac{1}{2} S_{\mathrm{I,II}} \left(E_{\mathrm{I}}^{\mathrm{corr}} + E_{\mathrm{II}}^{\mathrm{corr}} \right) \\ &= \langle \Psi_{\mathrm{I}} | \hat{H}_{\mathrm{NEO}} | \Psi_{\mathrm{II}} \rangle + \frac{1}{2} S_{\mathrm{I,II}} \left(E_{\mathrm{I}}^{\text{NEO-DFT}} - E_{\mathrm{I}}^{\text{NEO-HF}} + E_{\mathrm{II}}^{\text{NEO-DFT}} - E_{\mathrm{II}}^{\text{NEO-HF}} \right) \end{aligned} \tag{4}$$

Here $\langle \Psi_{\mathrm{I}} | \hat{H}_{\mathrm{NEO}} | \Psi_{\mathrm{II}} \rangle$ is computed at the NEO Hartree-Fock level with the NEO Hamiltonian $\hat{H}_{\mathrm{NEO}}$ using the Kohn-Sham orbitals for states I and II. The NEO Hamiltonian includes the kinetic energies of the electrons and quantum nuclei, as well as all Coulombic interactions. The correlation energy $E_{\mathrm{I}}^{\mathrm{corr}}$ or $E_{\mathrm{II}}^{\mathrm{corr}}$ is expressed as the difference between the NEO-DFT and NEO-HF energies for state I or II, respectively, as indicated. The analytical expressions for the NEO-MSDFT ground and excited states can then be expressed as:

$$
\begin{aligned}
E_0 &= \frac{1}{1-S_{\mathrm{I,II}}^2}\left[\frac{H_{\mathrm{I,I}}+H_{\mathrm{II,II}}-2S_{\mathrm{I,II}}H_{\mathrm{I,II}}-\sqrt{M}}{2}\right] \\
E_1 &= \frac{1}{1-S_{\mathrm{I,II}}^2}\left[\frac{H_{\mathrm{I,I}}+H_{\mathrm{II,II}}-2S_{\mathrm{I,II}}H_{\mathrm{I,II}}+\sqrt{M}}{2}\right] \\
M &= (H_{\mathrm{I,I}}-H_{\mathrm{II,II}})^2(1-S_{\mathrm{I,II}}^2)+\left[2H_{\mathrm{I,II}}-(H_{\mathrm{I,I}}+H_{\mathrm{II,II}})S_{\mathrm{I,II}}\right]^2
\end{aligned}
\tag{5}
$$

To account for the limitations of the electron-proton correlation functional and the associated inaccuracies in the overlap between the two localized nuclear-electronic wave functions,[33] we applied a correction to the overlap term $S_{\mathrm{I,II}}$ such that $S'_{\mathrm{I,II}} = \alpha(S_{\mathrm{I,II}})^{\beta}$ where α = 0.0604 and β = 0.492. This correction function was parameterized for a small model system and was subsequently verified to be transferrable and effective for predicting accurate tunneling splittings of five different molecular systems with different geometries.[33] We denoted this modified NEO-MSDFT method with the corrected overlap term as NEO-MSDFT′ and will use this method across all the simulations in this paper without the prime for notational simplicity. Recently, we also implemented the analytical gradients of the NEO-MSDFT ground and excited vibronic state energies and applied them to geometry optimizations and the generation of minimum energy paths for different molecular systems.[33]

2.2. Adiabatic, Ehrenfest, and surface hopping dynamics with NEO-MSDFT

In this subsection, we present details of the NEO-MSDFT adiabatic and nonadiabatic Ehrenfest, and surface hopping dynamics simulations. Herein, the ground and first excited adiabatic NEO-MSDFT vibronic states are denoted $\psi_0(\mathbf{r}^{\mathrm{e}},\mathbf{r}^{\mathrm{p}};\mathbf{R})$ and $\psi_1(\mathbf{r}^{\mathrm{e}},\mathbf{r}^{\mathrm{p}};\mathbf{R})$, respectively, which have energies E_0 and E_1 given in Eq. (5) and depend parametrically on the classical nuclear coordinates **R**. For adiabatic dynamics, the classical nuclei are propagated according to Newton's equations of motion on the NEO-MSDFT ground vibronic state:

$$M_I \ddot{\mathbf{R}}_I(t) = -\nabla_{\mathbf{R}_I} \left\langle \psi_0(\mathbf{r}^{\mathrm{e}}, \mathbf{r}^{\mathrm{p}}; \mathbf{R}) \,|\, \hat{H}_{\mathrm{NEO}} \,|\, \psi_0(\mathbf{r}^{\mathrm{e}}, \mathbf{r}^{\mathrm{p}}; \mathbf{R}) \right\rangle = -\nabla_{\mathbf{R}_I} E_0 \tag{6}$$

where M_I and $\mathbf{R}_I$ denote the mass and coordinates of the classic nucleus I.

For Ehrenfest dynamics, the time-dependent wave function $\Psi(\mathbf{r}^{\mathrm{e}}, \mathbf{r}^{\mathrm{p}}, t; \mathbf{R})$ is expanded in the basis of NEO-MSDFT adiabatic vibronic states:

$$\Psi(\mathbf{r}^{\mathrm{e}}, \mathbf{r}^{\mathrm{p}}, t; \mathbf{R}) = C_0(t)\psi_0(\mathbf{r}^{\mathrm{e}}, \mathbf{r}^{\mathrm{p}}; \mathbf{R}) + C_1(t)\psi_1(\mathbf{r}^{\mathrm{e}}, \mathbf{r}^{\mathrm{p}}; \mathbf{R}) \tag{7}$$

The classical nuclei are propagated on the average vibronic surface determined by this time-dependent wavefunction, leading to the following equations of motion:

$$\begin{aligned} M_I \ddot{\mathbf{R}}_I(t) &= -\nabla_{\mathbf{R}_I} \left\langle \Psi(\mathbf{r}^{\mathrm{e}}, \mathbf{r}^{\mathrm{p}}, t; \mathbf{R}) \,|\, \hat{H}_{\mathrm{NEO}} \,|\, \Psi(\mathbf{r}^{\mathrm{e}}, \mathbf{r}^{\mathrm{p}}, t; \mathbf{R}) \right\rangle \\ &= -\sum_{i=0,1} \sum_{j=0,1} C_i^* C_j \left\langle \psi_i(\mathbf{r}^{\mathrm{e}}, \mathbf{r}^{\mathrm{p}}; \mathbf{R}) \,|\, \nabla_{\mathbf{R}_I} \hat{H}_{\mathrm{NEO}} \,|\, \psi_j(\mathbf{r}^{\mathrm{e}}, \mathbf{r}^{\mathrm{p}}; \mathbf{R}) \right\rangle \end{aligned} \tag{8}$$

In the summation, the diagonal terms (i.e., $i = j$) are the gradients of the NEO-MSDFT ground and excited vibronic state energies, E_0 and E_1, respectively. Analytical expressions for these gradients are provided in Ref. 38. The off-diagonal term (i.e., $i \neq j$) are related to the nonadiabatic coupling vector $\mathbf{d}_{ij}$ as follows:

$$\mathbf{d}_{ij} = \left\langle \psi_i(\mathbf{r}^{\mathrm{e}}, \mathbf{r}^{\mathrm{p}}) \,|\, \nabla_{\mathbf{R}} \psi_j(\mathbf{r}^{\mathrm{e}}, \mathbf{r}^{\mathrm{p}}) \right\rangle = \frac{\left\langle \psi_i(\mathbf{r}^{\mathrm{e}}, \mathbf{r}^{\mathrm{p}}) \,|\, \nabla_{\mathbf{R}} \hat{H}_{\mathrm{NEO}} \,|\, \psi_j(\mathbf{r}^{\mathrm{e}}, \mathbf{r}^{\mathrm{p}}) \right\rangle}{E_j - E_i} \tag{9}$$

Here and in other equations below, the parametric dependence of the NEO-MSDFT vibronic states on $\mathbf{R}$ is not included for notational simplicity. The explicit expression for the nonadiabatic coupling vector $\mathbf{d}_{ij}$ is given in the Supporting Information (SI).

The time-dependent coefficients, $C_0(t)$ and $C_1(t)$, are determined by propagating the time-dependent Schrödinger equation

$$i\hbar \frac{\partial}{\partial t} \Psi(\mathbf{r}^{\mathrm{e}}, \mathbf{r}^{\mathrm{p}}, t) = \hat{H}_{\mathrm{NEO}} \Psi(\mathbf{r}^{\mathrm{e}}, \mathbf{r}^{\mathrm{p}}, t) \tag{10}$$

Substituting Eq. (7) into Eq. (10) leads to the following expression:

$$\dot{C}_j(t) = -\sum_{i=0,1} C_i(t)\left(\left\langle \psi_j \left| \frac{\partial \psi_i}{\partial t} \right\rangle + \frac{i}{\hbar} E_i \delta_{ij}\right)\right. \tag{11}$$

The nonadiabatic coupling element can be expressed in terms of the nonadiabatic coupling vector $\mathbf{d}_{ij}$ and the velocity vector $\mathbf{v}$ as

$$\left\langle \psi_j \left| \frac{\partial \psi_i}{\partial t} \right\rangle = \mathbf{d}_{ij} \cdot \mathbf{v} \right. \tag{12}$$

To avoid numerical instabilities and ensure accuracy even when the nonadiabatic coupling element exhibits sharp peaks,[48] we computed this matrix element with the numerical finite difference method:[39]

$$\left\langle \psi_j(t+\Delta t/2) \left| \frac{\partial \psi_i(t+\Delta t/2)}{\partial t} \right\rangle \right. \approx \frac{1}{2\Delta t}\left[\left\langle \psi_j(t) \,|\, \psi_i(t+\Delta t)\right\rangle - \left\langle \psi_j(t+\Delta t) \,|\, \psi_i(t)\right\rangle\right] \tag{13}$$

We also implemented the norm-preserving interpolation method of Meek and Levine[48] and showed that the results obtained with this method are consistent with the results obtained using Eq. (13) (see Figure S3). Note that this approach approximates the wave function in the framework of the Kohn-Sham formalism, similar to nonadiabatic dynamics treatments with conventional electronic TDDFT.

We also explored surface hopping dynamics on the NEO-MSDFT adiabatic vibronic state surfaces. In this case, the nuclei evolve on a single adiabatic NEO-MSDFT vibronic state surface *k* according to

$$M_I \ddot{\mathbf{R}}_I(t) = -\nabla_{\mathbf{R}_I}\left\langle \psi_k(\mathbf{r}^e, \mathbf{r}^p; \mathbf{R}) \,|\, \hat{H}_{\mathrm{NEO}} \,|\, \psi_k(\mathbf{r}^e, \mathbf{r}^p; \mathbf{R})\right\rangle = -\nabla_{\mathbf{R}_I} E_k \tag{14}$$

Typically instantaneous transitions between adiabatic surfaces are incorporated according to a stochastic algorithm based on the quantum amplitudes $C_0(t)$ and $C_1(t)$, which are determined by

integrating Eq. (11). To obtain statistically meaningful results from a surface hopping method such as Tully's fewest switching algorithm,[43] a large number of independent trajectories must be propagated. For the purposes of demonstrating surface hopping with NEO-MSDFT, we used an alternative approach to avoid propagating a large number of trajectories. Specifically, we propagated a small set of trajectories and used the Landau-Zener (LZ) formula to estimate the nonadiabatic transition probability[49] and determine when the transitions should occur. Within this context, the LZ transition probability between the adiabatic vibronic states 0 and 1 in the vicinity of an avoided crossing can be expressed as[49]

$$P = \exp\left(-\frac{2\pi V_{\mathrm{I,II}}^2}{|\nabla_{\mathbf{R}} E_{\mathrm{II}} - \nabla_{\mathbf{R}} E_{\mathrm{I}}| \cdot \mathbf{v}} \right) \tag{15}$$

where E_{I} and E_{II} are the energies of the approximate diabatic states (i.e., the localized NEO-DFT states) and $V_{\mathrm{I,II}}$ is the vibronic coupling between the approximate diabatic states expressed as

$$V_{\mathrm{I,II}} = \frac{1}{1 - S_{\mathrm{I,II}}^2} \left| H_{\mathrm{I,II}} - \frac{H_{\mathrm{I,I}} + H_{\mathrm{II,II}}}{2} S_{\mathrm{I,II}} \right| \tag{16}$$

Note that Eq. (15) is valid only in the avoided crossing regions. When a transition occurs, to maintain energy conservation, the velocities are adjusted according to a force in the direction of the nonadiabatic coupling vector.[39]

In our simulations, the nonadiabatic transitions were considered to occur at the local maxima of the LZ transition probability within the avoided crossing regions between the vibronic surfaces. As will be shown below, proton transfer in malonaldehyde exhibits two distinct avoided crossing regions. Four trajectories were propagated to sample the four distinct pathways, and the LZ transition probabilities were used to weight these trajectories in a manner that provides a reasonable estimate of the proton transfer time.

2.3. Computational details

The NEO-MSDFT method has been implemented in a developer version of Q-Chem 5.3[50] to enable calculation of the energies,[33] analytical gradients,[38] and analytical nonadiabatic coupling vectors. The expression for the analytical nonadiabatic coupling vector is given in the SI. All the NEO-MSDFT dynamics simulations were carried out using our in-house code with an interface connecting to Q-Chem. We chose malonaldehyde as a prototypical molecular system exhibiting hydrogen tunneling[24-26, 45-47] to illustrate adiabatic, Ehrenfest, and surface hopping dynamics simulations. The same initial conditions were applied to all dynamics simulations, where each trajectory starts from the NEO-MSDFT ground state equilibrium structure of malonaldehyde. The initial velocities for the classical nuclei were assigned in the direction from the equilibrium geometry toward the transition state geometry with a total kinetic energy corresponding to 150 K.

We applied the fourth-order Runge-Kutta numerical integration method to integrate Eq. (11), which typically requires a smaller time step than the time step Δt required to integrate the classical equations of motion (Eq. (8)). The nonadiabatic coupling elements were linearly interpolated between $t - \Delta t/2$ to $t + \Delta t/2$, and the NEO-MSDFT vibronic state energies were linearly interpolated between t and $t + \Delta t$. The integration time step was 0.15 fs for the classical equations of motion and 0.0003 fs for the time-dependent Schrödinger equation.

Within the NEO-MSDFT framework, we used the B3LYP electronic density functional[51-52] and the epc17-2 electron-proton correlation functional,[10] together with the cc-pVTZ electronic basis set[53] and the PB4-D protonic basis set.[54] For each malonaldehyde geometry at each time step, the transferring proton is represented by two basis function centers that are optimized variationally. Each basis function center is positioned near either the donor or the acceptor oxygen and contains

a set of electronic and protonic basis functions. To accelerate the optimization process at each time step, first each of the two proton basis function centers was optimized separately for each localized NEO-DFT state, and subsequently the two proton basis function centers were optimized simultaneously on the specified adiabatic vibronic surface. This basis function center optimization procedure was performed on the NEO-MSDFT ground vibronic state surface for adiabatic dynamics, on the occupied vibronic state surface for surface hopping dynamics, and on either the ground or mixed vibronic state surface for Ehrenfest dynamics, where these two strategies were shown to produce similar results (see Figure S4). In some proton transfer reactions, the double-well potential energy surface can change to a single-well potential energy surface. In this case, the two basis function centers should smoothly optimize variationally toward the minimum while remaining sufficiently separated to avoid linear dependencies. In some dynamical trajectories, however, numerical issues may be encountered if the change occurs over an extremely short time period, and a smaller time step is required to ensure numerical stability.

The most computationally intensive parts of these calculations are the optimization of the basis function center positions at each time step, which could be avoided using traveling basis functions,[23] and the solution of the coupled-perturbed NEO-SCF equations to compute the analytical gradients and nonadiabatic coupling vectors. The current NEO-MSDFT nonadiabatic dynamics code has not been optimized yet for computational efficiency.

The current implementation of the NEO-MSDFT approach is qualitatively but not necessarily quantitatively accurate for dynamical simulations (see Figure S2). Moreover, the vibronic states associated with the bending modes of the transferring hydrogen are not included in the two-state NEO-MSDFT implementation. The proton densities associated with these bending modes can be computed with NEO-TDDFT or grid-based methods, and they have been found to

be mainly perpendicular to the proton densities associated with the stretching modes.[55] These vibronic states are not expected to couple strongly to the vibronic states of interest for hydrogen tunneling. However, the approach could be extended to include additional vibronic states if needed.

The extension to multiple proton transfer reactions is more straightforward. The description of multiple proton transfer reactions requires two proton basis function centers per transferring proton and up to 2^N localized NEO-DFT states to construct the nonorthogonal configuration interaction matrix for N transferring protons. When more vibronic states are included, the matrix equation given by Eq. (1) can be solved using a standard linear algebra library. This framework allows the proton configurations to change along the reaction pathway.

3. Results and Discussion

3.1. Adiabatic ground state dynamics

In this subsection, we present the results from an adiabatic dynamics trajectory on the NEO-MSDFT ground vibronic state. In this case, the proton density, as well as the electron density, responds instantaneously to the movement of the classical nuclei. Figure 1A shows configurations of the classical nuclei as well as isosurface plots of the quantum proton density along the trajectory. Similar to our previous investigation using smaller electronic/protonic basis sets,[15] the NEO-MSDFT ground state trajectory for malonaldehyde shows the proton density evolving from being localized near the donor oxygen to being delocalized between the two oxygen atoms and finally being localized near the acceptor oxygen. In the conventional Born-Oppenheimer picture, the asymmetric, bilobal proton densities at 6, 10, and 15 fs correspond to a slightly asymmetric double-well potential energy surface, while the single-lobe but slightly delocalized proton density at 12 fs

corresponds to the ground proton vibrational state above the barrier on a more symmetric surface. As expected, the distance between the donor and acceptor oxygen atoms is a minimum at ~12 fs.

Figure 1B presents the distances from the expectation value of the quantum proton position to the donor oxygen and the acceptor oxygen along the trajectory. Consistent with the movement of the quantum proton density shown in Figure 1A, the expectation value of the quantum proton position moves away from the donor oxygen and toward the acceptor oxygen. The quantum proton is equidistant between the donor and acceptor oxygen atoms (i.e., the red and blue lines cross in Figure 1B) at ~12 fs, which we denote the proton transfer time for simplicity. Note that for systems exhibiting recrossings in this region, a more robust definition of the proton transfer time would be the time required for the proton to form a covalent bond with the acceptor.[39] At ~19 fs, the proton reaches the closest position relative to the acceptor proton and starts to move back toward the donor oxygen.

The driving force for proton transfer is mainly the movement of the two C–O groups that bracket the quantum proton. Starting from the equilibrium structure of malonaldehyde, the C–O bond involving the donor oxygen decreases in length, while the other C–O bond involving the acceptor oxygen increases in length. At ~12 fs, the configuration of the molecule is close to the transition state geometry,[38] where the two C–O bond lengths are similar. After this time, the C–O bond involving the donor oxygen continues to decrease, and the quantum proton continues to transfer to the acceptor oxygen. The donor and acceptor oxygen atoms also move toward each other until ~12 fs and then move apart again as the trajectory continues. These results agree with the qualitative characteristics of the minimum energy path on the NEO-MSDFT ground vibronic state surface.[38]

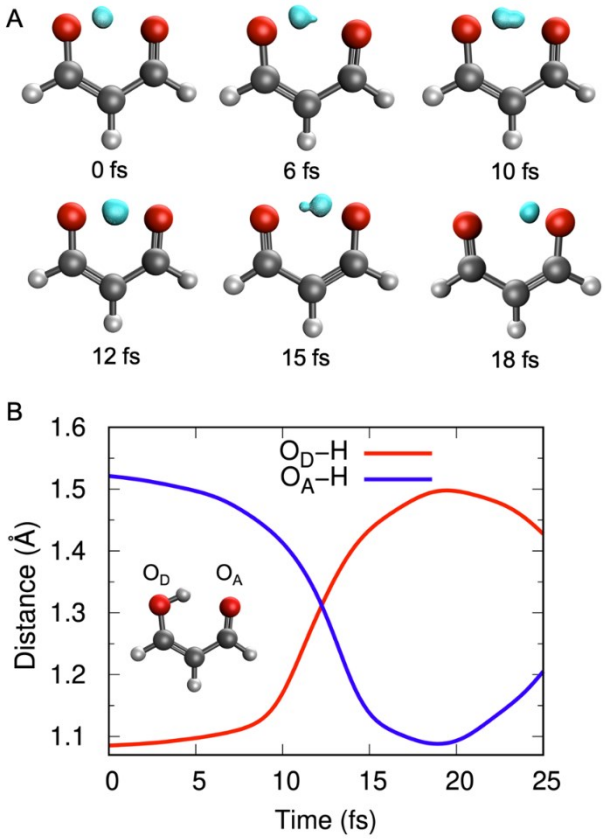

Figure 1. Adiabatic dynamics trajectory on the NEO-MSDFT ground vibronic state surface for malonaldehyde. (A) Configurations along the trajectory, where the quantum proton density is plotted in cyan with an isosurface value of 0.02. (B) Distance from the expectation value of the transferring proton position to the donor oxygen (O_D) and the acceptor oxygen (O_A) as a function of time along the trajectory.

3.2. Ehrenfest dynamics

Although the adiabatic dynamics trajectory on the NEO-MSDFT ground vibronic state surface provides a clear picture of intramolecular proton transfer in malonaldehyde, it neglects the contribution from the excited vibronic state, which can be important due to the small splitting between the ground and excited vibronic states. Nonadiabatic dynamics approaches are needed to provide a more accurate description of this type of process. One such approach is based on Ehrenfest dynamics, where the classical nuclei move on a mean-field or average potential energy surface. We combined the NEO-MSDFT method with Ehrenfest dynamics to propagate the classical nuclei on a vibronic surface that is a linear combination of the ground and excited state

vibronic surfaces. The solid lines in Figure 2A represent the distances between the expectation value of the transferring proton position and the donor and acceptor oxygen atoms obtained from an Ehrenfest dynamics trajectory. The general features of the proton transfer process are similar to those observed in the adiabatic ground state dynamics trajectory (dashed lines in Figure 2A). The main difference between the Ehrenfest and adiabatic trajectories is that the quantum proton transfers slower for the Ehrenfest dynamics trajectory. The proton transfer time is ~17 fs in the Ehrenfest dynamics trajectory compared to ~12 fs in the adiabatic trajectory. The involvement of the excited vibronic state slows down the movement of the classical nuclei, especially the change of the two C–O bond lengths and the decrease of the O–O distance, and thereby slows down proton transfer.

To understand this behavior, we need to track the role of the NEO-MSDFT excited vibronic state along the trajectory. Figure 2B provides the quantum probabilities, C_0^2 and C_1^2, for the NEO-MSDFT ground and excited vibronic states as a function of time along the Ehrenfest dynamics trajectory. In the first 5 fs of the trajectory, the quantum probability of the excited state, C_1^2, is almost 0, and therefore the trajectory is propagated almost purely on the ground vibronic state surface within this time interval (solid and dashed lines are identical in Figure 2A). After 5 fs, C_1^2 begins to increase, and the NEO-MSDFT excited vibronic state contributes more to the average vibronic surface. At ~15 fs, the weight of the excited vibronic state reaches its maximum and is slightly higher than the weight of the ground vibronic state. After 15 fs, C_1^2 begins to decrease and reaches a local minimum at ~17 fs and increases again until ~21 fs. After 21 fs, C_1^2 decreases as the time-dependent wavefunction becomes almost entirely dominated by the ground vibronic state, and the transferring proton is localized on the acceptor oxygen. The nonadiabatic coupling element, $\langle \psi_0 | \partial \psi_1 / \partial t \rangle$, also exhibits peaks in the regions of 15 and 21 fs, as shown in Figure 2C.

This behavior of the quantum probabilities and nonadiabatic coupling can be understood in the context of the minimum energy path generated on the NEO-MSDFT ground vibronic state and the corresponding energies of the excited vibronic state for the geometries along this pathway (Figure S1). For configurations close to the equilibrium structure, the excited vibronic state energy is significantly higher than the ground vibronic state energy because the quantum proton is localized near the donor oxygen (see the proton density in Figure S1). At the transition state geometry, the quantum proton is a single delocalized lobe equidistant from the donor and acceptor oxygen atoms (see the proton density in Figure S1). Because of the relatively short oxygen-oxygen distance at the transition state, the splitting between the ground and excited vibronic states at this geometry is relatively large. In the conventional Born-Oppenheimer picture, the barrier at the transition state is so low that the proton vibrational ground state is above the barrier (see the symmetric proton potential in Figure S1). In contrast, symmetric configurations obtained by averaging the reactant and product structures lead to significantly smaller tunneling splittings for malonaldehyde, as shown in Ref. [33] for both the NEO-MSDFT method and a numerically exact grid-based method, but such conformations are not sampled along the minimum energy path or along trajectories generated at relatively high temperatures. Most interestingly, in the regions between the equilibrium and transition state structures, the energy difference between the NEO-MSDFT excited and ground vibronic states is very small. In the conventional Born-Oppenheimer picture, the proton is moving on a slightly asymmetric double well potential energy surface (see corresponding proton potential in Figure S1). The resulting proton density is bilobal and slightly asymmetric in both the ground and excited vibronic states (see the proton densities in Figure S1), corresponding to a small energy splitting. There are two such regions, one on each side of the transition state, due to the symmetry of malonaldehyde.

Similar behavior is observed along the Ehrenfest dynamics trajectory, as shown by the proton densities of the ground and excited vibronic states at the regions of strong nonadiabatic coupling (i.e., 15 fs and 21 fs in Figure 2D). At the start of the trajectory, the proton density is localized near the donor oxygen, but at 15 fs, the proton density becomes delocalized, bilobal, and slightly asymmetric, corresponding to a region of strong nonadiabatic coupling. The proton density becomes more symmetric with a single lobe at ~17 fs, but then becomes bilobal and slightly asymmetric again at ~21 fs, corresponding to another region of strong nonadiabatic coupling. These two regions of strong nonadiabatic coupling are related to the two regions with small energy splitting on each side of the transition state along the minimum energy path (Figure S1). As the trajectory progresses, the proton density becomes localized on the acceptor oxygen, where the nonadiabatic coupling is negligible. These proton densities are qualitatively similar to those plotted along the minimum energy path (Figure S1). The contribution from the excited vibronic state slows down proton transfer because it increases the energy barrier along the trajectory. Similar behavior is illustrated by the minimum energy path in Figure S1: the barrier along the minimum energy path is clearly higher for a mixture of the ground and excited vibronic states than the ground vibronic state.

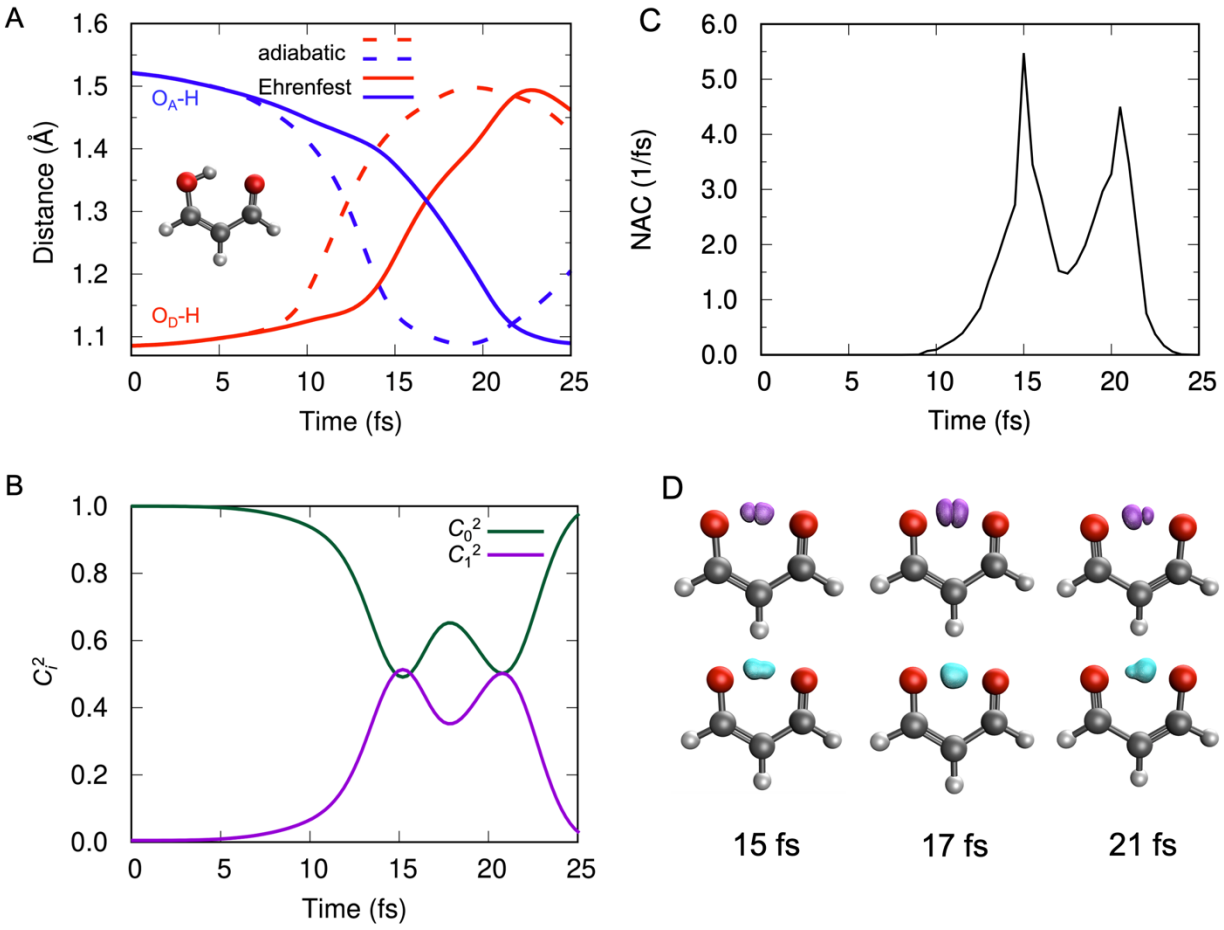

Figure 2. Ehrenfest dynamics trajectory on the NEO-MSDFT vibronic surfaces for malonaldehyde. (A) Distance from the expectation value of the transferring proton position to the donor oxygen (O_D) and the acceptor oxygen (O_A) as a function of time from an Ehrenfest dynamics trajectory (solid lines) and an adiabatic ground vibronic state trajectory (dashed lines, same as Figure 1B). (B) Quantum probabilities C_0^2 and C_1^2 associated with the NEO- MSDFT ground and excited vibronic states, respectively, along the Ehrenfest dynamics trajectory. (C) Nonadiabatic coupling element (NAC) along the Ehrenfest dynamics trajectory. (D) Configurations at 15 fs, 17 fs, and 21 fs with the quantum proton density plotted in cyan for the ground vibronic state and in purple for the excited vibronic state.

Including the effects of the NEO-MSDFT excited vibronic state via Ehrenfest dynamics has been shown to influence the proton transfer process in malonaldehyde and to decrease the proton transfer rate. A well-known limitation of Ehrenfest dynamics, however, is that it is unable to describe branching processes, where two potential energy surfaces exhibit distinct forces after a region of strong nonadiabatic coupling. Proton transfer is known to exhibit such branching

processes.[39] An alternative nonadiabatic dynamics approach, surface hopping, is able to describe branching processes by propagating on adiabatic potential energy surfaces with instantaneous transitions incorporated in a manner that reflects the quantum probabilities determined by integration of the time-dependent Schrödinger equation. As mentioned above, the fewest switches surface hopping method[43] requires the propagation of a large ensemble of trajectories to obtain reliable results. Given the distinct localized regions of strong nonadiabatic coupling shown in Figure 2B and 2C, we employed an alternative strategy based on the Landau-Zener probability to avoid this computational expense.

3.3. Surface hopping dynamics

To demonstrate NEO-MSDFT with surface hopping dynamics, we propagated four representative trajectories corresponding to the four cases of a transition occurring or not occurring at each of the two distinct avoided crossing regions (i.e., strong nonadiabatic coupling regions). A nonadiabatic transition was incorporated when the Landau-Zener probability, given in Eq. (15), reached a local maximum within an avoided crossing region. Figure 3 and Figure 4 show the simulation results from two different representative surface hopping trajectories.

For the trajectory shown in Figure 3, two nonadiabatic transitions occur, with the first transition at 9.6 fs and the second transition at 20.2 fs, corresponding to the two local maxima in the Landau-Zener probability in these regions. Prior to 9.6 fs, the classical nuclei move on the NEO-MSDFT ground vibronic state surface, and the trajectory is identical to the previous adiabatic ground vibronic state trajectory (dashed lines in Figure 3). After the first transition at 9.6 fs, the nuclei move on the NEO-MSDFT excited vibronic state surface, which slows down proton transfer for similar reasons as discussed above for the Ehrenfest dynamics trajectory. Specifically, the barrier to proton transfer is higher on the excited state surface. Thus, the trajectory requires an

additional 9.3 fs to reach the point where the expectation value of the quantum proton is equidistant from the donor and acceptor oxygen atoms. The classical nuclei continue to move on the excited vibronic state surface until the second transition at 20.2 fs, when the nuclei start moving on the ground vibronic state surface, and the expectation value of the quantum proton continues to approach the acceptor oxygen. Figure 3B depicts the quantum probabilities for the ground and excited vibronic states. If enough independent trajectories were generated with Tully's fewest switches algorithm,[43] the fraction of trajectories in a given state i at time t would be C_i^2, except for complications associated with classically forbidden transitions.

Figure 4 shows another example of a surface hopping trajectory, where a nonadiabatic transition did not occur at 9.6 fs, even though the Landau-Zener probability reaches a maximum. This trajectory continues to move on the NEO-MSDFT ground vibronic state and is identical to the adiabatic ground vibronic state trajectory (dashed lines in Figure 4) until 15.5 fs. At this time, the Landau-Zener probability reaches the second maximum, and a nonadiabatic transition to the excited vibronic state occurs. As seen in Figure 4A, however, the crossing between the two curves (solid red and blue lines) associated with proton transfer occurred at 12.3 fs, which was prior to the nonadiabatic transition. Such a surface hopping trajectory does not affect the proton transfer rate when it is defined to be the time at which the expectation value of the transferring proton position is equidistant from the donor and acceptor oxygen atoms. We also investigated other types of surface hopping trajectories: (1) no hop allowed along the trajectory and (2) only one hop allowed at 9.6 fs. The first case (Figure S5) is identical to the adiabatic ground state trajectory. For the second case (Figure S6), the trajectory is similar to the one with two nonadiabatic transitions shown in Figure 3 and exhibits an identical proton transfer rate. The slight difference occurs after 20.2 fs, when the trajectory shown in Figure 3 allows a nonadiabatic transition back down to the

ground vibronic state surface, while the trajectory shown in Figure S6 remains on the excited vibronic state surface.

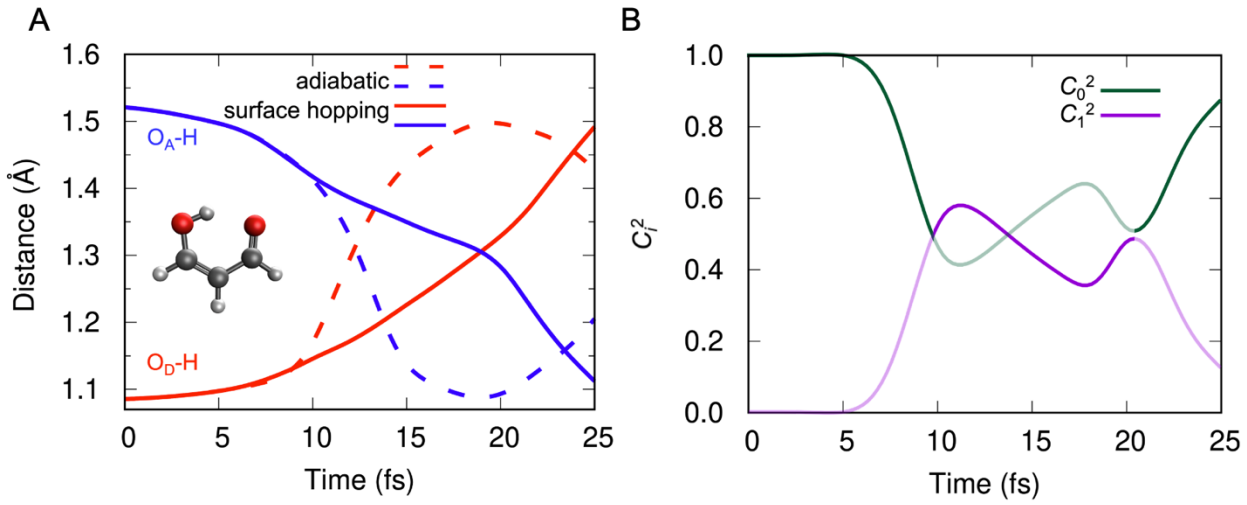

Figure 3. Representative surface hopping dynamics trajectory on the NEO-MSDFT vibronic surfaces for malonaldehyde. (A) Distance from the expectation value of the transferring proton position to the donor oxygen (O_D) and the acceptor oxygen (O_A) as a function of time from a representative surface hopping trajectory (solid lines) and an adiabatic ground vibronic state trajectory (dashed lines, same as Figure 1B). (B) Quantum probabilities C_0^2 and C_1^2 associated with the NEO-MSDFT ground and excited vibronic states, respectively, along the surface hopping trajectory (darker line shows occupied state, where the first transition occurs at 9.6 fs and the second transition occurs at 20.2 fs).

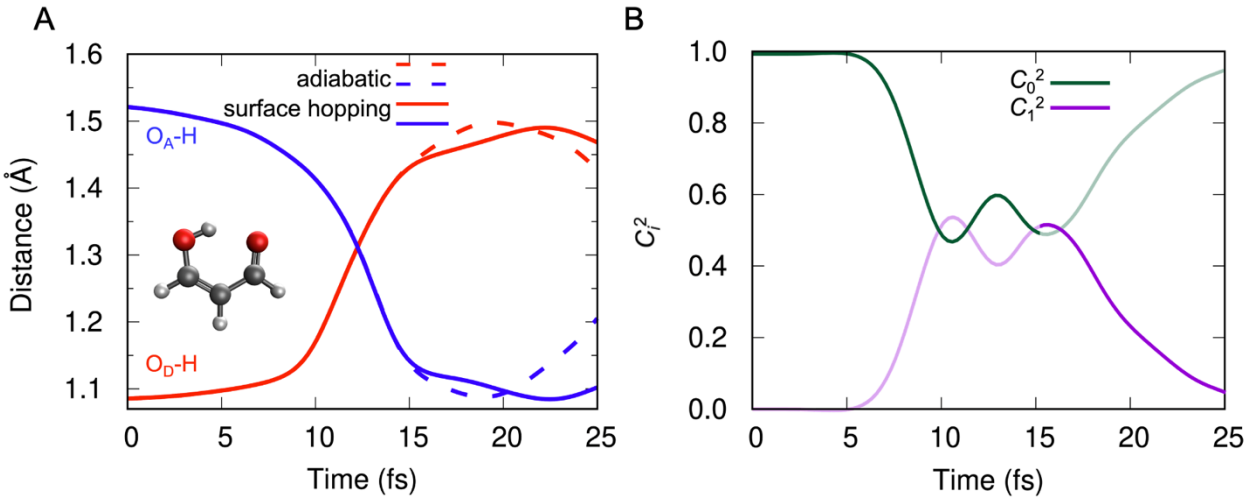

Figure 4. Representative surface hopping dynamics trajectory on the NEO-MSDFT vibronic surfaces for malonaldehyde. (A) Distance from the expectation value of the transferring proton position to the donor oxygen (O_D) and the acceptor oxygen (O_A) as a function of time from a representative surface hopping trajectory (solid lines) and an adiabatic ground vibronic state

trajectory (dashed lines, same as Figure 1B). (B) Quantum probabilities C_0^2 and C_1^2 associated with the NEO-MSDFT ground and excited vibronic states, respectively, along this surface hopping trajectory (darker line shows occupied state, where the transition occurs at 15.5 fs).

3.4. Combined analysis

Table 1 provides the proton transfer time obtained from the adiabatic, Ehrenfest, and surface hopping dynamics simulations with the same initial conditions. Here, the proton transfer time is defined as the time when the expectation value of the quantum proton position is equidistant to the donor and acceptor oxygen atoms. As discussed above, the adiabatic ground vibronic state trajectory predicts the fastest proton transfer time of 12.3 fs. The Ehrenfest dynamics trajectory, which includes contributions from the excited vibronic state associated with a higher barrier for proton transfer, delays the time for proton transfer to 16.9 fs. For the surface hopping trajectories, we estimated the proton transfer time using the four representative trajectories. Two of these trajectories exhibit a proton transfer time of 18.8 fs, where the nonadiabatic transition occurs at 9.6 fs with a Landau-Zener probability of 0.72. The other two trajectories exhibit a proton transfer time of 12.3 fs, where a nonadiabatic transition does not occur at 9.6 fs or at any time before the proton transfers. To estimate the proton transfer time, we computed the weighted sum of these two proton transfer times using the Landau-Zener probability. This estimate results in a proton transfer time of 17.0 fs, which is very close to the Ehrenfest dynamics result for this specific system and set of initial conditions. It is important to note that a comparison to experimental measurements would require sampling over initial conditions.

Table 1. Proton Transfer Time[a] in Malonaldehyde from Different Dynamics Approaches

Approach	Time (fs)
adiabatic ground state	12.3
Ehrenfest	16.9
Surface hopping	17.0[b]

[a]The proton transfer time is defined as the time when the expectation value of the transferring proton position is equidistant to the donor and acceptor oxygen atoms. This proton transfer time is not comparable to experimental measurements because only a single set of initial conditions is considered.
[b]Estimated from a weighted sum of four independent trajectories using the Landau-Zener transition probability.

We also analyzed energy conservation for all of these trajectories. Figure S7 presents some examples, including the adiabatic ground state trajectory, the Ehrenfest dynamics trajectory, and one surface hopping trajectory. For the adiabatic ground state trajectory, the total energy exhibits excellent conservation with fluctuations within 2.0×10^{-5} Hartree. Energy conservation is not quite as good for the Ehrenfest and surface hopping dynamics trajectories, where the total energy deviation increases to ~6.0×10^{-5} Hartree. Such energy conservation behavior is considered to be acceptable in most situations and can be improved systematically using a tighter gradient tolerance for the basis function center optimization at each classical MD time step, as well as a smaller MD time step. This improvement is shown in Figure S8 for the HCN molecule. Similarly, for the current study of malonaldehyde, the total energy will be conserved better if a tighter gradient tolerance and smaller time step are used.

4. Conclusions

In this paper, we introduced a scheme combining the NEO-MSDFT approach with both adiabatic and nonadiabatic dynamics simulations of proton transfer reactions. Using malonaldehyde as a prototypical proton transfer system exhibiting hydrogen tunneling, we performed nonadiabatic Ehrenfest and surface hopping dynamics on the NEO-MSDFT vibronic state surfaces. The proton transfer process is analyzed by tracking the expectation value of the quantum proton position as well as the proton density. Upon inclusion of contributions from the excited vibronic state via either Ehrenfest or surface hopping dynamics, the proton transfer process is slowed down. In all cases, the total energy is well conserved, and energy conservation is shown to be further improved when a tighter gradient tolerance is used for optimizing the proton basis function centers.

In prior work, the NEO-MSDFT approach was shown to produce quantitatively accurate hydrogen tunneling splittings for fixed geometries.[33] The combination of the NEO-MSDFT approach with nonadiabatic dynamics methods opens up new possibilities for investigating hydrogen tunneling dynamics at finite temperature, while including the coupling between the transferring hydrogen and the other nuclei. Comparison to experimental data obtained at these temperatures will require the simulation of a large number of nonadiabatic dynamics trajectories averaged over initial conditions that are consistent with the experimental conditions. Hydrogen tunneling splittings for comparison with experimental data can be calculated with methods such as vibronic coupling theory, as applied previously within the NEO framework.[46]

Attaining quantitative accuracy with these methods may require further improvement of the NEO-MSDFT scheme. Such improvements include the development of more accurate electron-proton correlation functionals and the addition of more vibronic states. Moreover, the

description of multiple proton transfer reactions will require additional vibronic states. These extensions represent future directions that will enable a wide range of hydrogen tunneling simulations.

Supporting Information

Derivation and benchmarking of NEO-MSDFT analytical nonadiabatic coupling vector; NEO-MSDFT ground and excited vibronic state energies and proton densities along minimum energy path; additional representative surface hopping trajectories; total energy conservation from adiabatic, Ehrenfest, and surface hopping dynamics trajectories; analysis of total energy conservation for HCN molecule.

Acknowledgement

The authors thank Dr. Alexander Soudackov, Prof. John Tully, Joseph Dickinson, Dr. Christopher Malbon, Dr. Tao Li, Dr. Jonathan Fetherolf, and Mathew Chow for useful discussions. This work was supported by the National Science Foundation Grant No. CHE-1954348.

Data Availability Statement

The data that support the findings of this study are available within the article and its Supporting Information.

References

1. Cha, Y.; Murray, C. J.; Klinman, J. P. Hydrogen Tunneling in Enzyme Reactions. *Science* **1989,** *243*, 1325-1330.
2. Richardson, J. O.; Pérez, C.; Lobsiger, S.; Reid, A. A.; Temelso, B.; Shields, G. C.; Kisiel, Z.; Wales, D. J.; Pate, B. H.; Althorpe, S. C. Concerted Hydrogen-Bond Breaking by Quantum Tunneling in the Water Hexamer Prism. *Science* **2016,** *351*, 1310.
3. Vaillant, C. L.; Wales, D. J.; Althorpe, S. C. Tunneling Splittings in Water Clusters from Path Integral Molecular Dynamics. *J. Phys. Chem. Lett.* **2019,** *10*, 7300-7304.
4. Litman, Y.; Richardson, J. O.; Kumagai, T.; Rossi, M. Elucidating the Nuclear Quantum Dynamics of Intramolecular Double Hydrogen Transfer in Porphycene. *J. Am. Chem. Soc.* **2019,** *141*, 2526-2534.
5. Gust, D.; Moore, T. A.; Moore, A. L. Solar Fuels Via Artificial Photosynthesis. *Acc. Chem. Res.* **2009,** *42*, 1890-1898.
6. Hammarström, L.; Styring, S. Proton-Coupled Electron Transfer of Tyrosines in Photosystem Ii and Model Systems for Artificial Photosynthesis: The Role of a Redox-Active Link between Catalyst and Photosensitizer. *Energy & Environmental Science* **2011,** *4*, 2379-2388.
7. Stubbe, J.; Nocera, D. G.; Yee, C. S.; Chang, M. C. Y. Radical Initiation in the Class I Ribonucleotide Reductase: Long-Range Proton-Coupled Electron Transfer? *Chem. Rev.* **2003,** *103*, 2167-2202.
8. Webb, S. P.; Iordanov, T.; Hammes-Schiffer, S. Multiconfigurational Nuclear-Electronic Orbital Approach: Incorporation of Nuclear Quantum Effects in Electronic Structure Calculations. *J. Chem. Phys.* **2002,** *117*, 4106-4118.
9. Pak, M. V.; Chakraborty, A.; Hammes-Schiffer, S. Density Functional Theory Treatment of Electron Correlation in the Nuclear−Electronic Orbital Approach. *J. Phys. Chem. A* **2007,** *111*, 4522-4526.
10. Brorsen, K. R.; Yang, Y.; Hammes-Schiffer, S. Multicomponent Density Functional Theory: Impact of Nuclear Quantum Effects on Proton Affinities and Geometries. *J. Phys. Chem. Lett.* **2017,** *8*, 3488-3493.
11. Yang, Y.; Schneider, P. E.; Culpitt, T.; Pavošević, F.; Hammes-Schiffer, S. Molecular Vibrational Frequencies within the Nuclear–Electronic Orbital Framework. *J. Phys. Chem. Lett.* **2019,** *10*, 1167-1172.
12. Zhao, L.; Wildman, A.; Tao, Z.; Schneider, P.; Hammes-Schiffer, S.; Li, X. Nuclear–Electronic Orbital Ehrenfest Dynamics. *J. Chem. Phys.* **2020,** *153*, 224111.
13. Pavošević, F.; Culpitt, T.; Hammes-Schiffer, S. Multicomponent Quantum Chemistry: Integrating Electronic and Nuclear Quantum Effects Via the Nuclear–Electronic Orbital Method. *Chem. Rev.* **2020,** *120*, 4222-4253.
14. Schneider, P. E.; Tao, Z.; Pavošević, F.; Epifanovsky, E.; Feng, X.; Hammes-Schiffer, S. Transition States, Reaction Paths, and Thermochemistry Using the Nuclear–Electronic Orbital Analytic Hessian. *J. Chem. Phys.* **2021,** *154*, 054108.
15. Tao, Z.; Yu, Q.; Roy, S.; Hammes-Schiffer, S. Direct Dynamics with Nuclear–Electronic Orbital Density Functional Theory. *Acc. Chem. Res.* **2021,** *54*, 4131-4141.
16. Xu, X.; Chen, Z.; Yang, Y. Molecular Dynamics with Constrained Nuclear Electronic Orbital Density Functional Theory: Accurate Vibrational Spectra from Efficient Incorporation of Nuclear Quantum Effects. *J. Am. Chem. Soc.* **2022,** *144*, 4039-4046.

17. Pavošević, F.; Culpitt, T.; Hammes-Schiffer, S. Multicomponent Coupled Cluster Singles and Doubles Theory within the Nuclear-Electronic Orbital Framework. *J. Chem. Theory Comput.* **2018,** *15*, 338-347.
18. Pavošević, F.; Rousseau, B. J. G.; Hammes-Schiffer, S. Multicomponent Orbital-Optimized Perturbation Theory Methods: Approaching Coupled Cluster Accuracy at Lower Cost. *J. Phys. Chem. Lett.* **2020,** *11*, 1578-1583.
19. Fajen, O. J.; Brorsen, K. R. Multicomponent Mp4 and the Inclusion of Triple Excitations in Multicomponent Many-Body Methods. *J. Chem. Phys.* **2021,** *155*, 234108.
20. Yang, Y.; Brorsen, K. R.; Culpitt, T.; Pak, M. V.; Hammes-Schiffer, S. Development of a Practical Multicomponent Density Functional for Electron-Proton Correlation to Produce Accurate Proton Densities. *J. Chem. Phys.* **2017,** *147*, 114113.
21. Yang, Y.; Culpitt, T.; Hammes-Schiffer, S. Multicomponent Time-Dependent Density Functional Theory: Proton and Electron Excitation Energies. *J. Phys. Chem. Lett.* **2018,** *9*, 1765-1770.
22. Zhao, L.; Tao, Z.; Pavošević, F.; Wildman, A.; Hammes-Schiffer, S.; Li, X. Real-Time Time-Dependent Nuclear−Electronic Orbital Approach: Dynamics Beyond the Born–Oppenheimer Approximation. *J. Phys. Chem. Lett.* **2020,** *11*, 4052-4058.
23. Zhao, L.; Wildman, A.; Pavošević, F.; Tully, J. C.; Hammes-Schiffer, S.; Li, X. Excited State Intramolecular Proton Transfer with Nuclear-Electronic Orbital Ehrenfest Dynamics. *J. Phys. Chem. Lett.* **2021,** *12*, 3497-3502.
24. Wang, Y.; Braams, B. J.; Bowman, J. M.; Carter, S.; Tew, D. P. Full-Dimensional Quantum Calculations of Ground-State Tunneling Splitting of Malonaldehyde Using an Accurate Ab Initio Potential Energy Surface. *J. Chem. Phys.* **2008,** *128*, 224314.
25. Hammer, T.; Coutinho-Neto, M. D.; Viel, A.; Manthe, U. Multiconfigurational Time-Dependent Hartree Calculations for Tunneling Splittings of Vibrational States: Theoretical Considerations and Application to Malonaldehyde. *J. Chem. Phys.* **2009,** *131*, 224109.
26. Schröder, M.; Gatti, F.; Meyer, H.-D. Theoretical Studies of the Tunneling Splitting of Malonaldehyde Using the Multiconfiguration Time-Dependent Hartree Approach. *J. Chem. Phys.* **2011,** *134*, 234307.
27. Pak, M. V.; Hammes-Schiffer, S. Electron-Proton Correlation for Hydrogen Tunneling Systems. *Phys. Rev. Lett.* **2004,** *92*, 103002.
28. Pak, M. V.; Swalina, C.; Webb, S. P.; Hammes-Schiffer, S. Application of the Nuclear-Electronic Orbital Method to Hydrogen Transfer Systems: Multiple Centers and Multiconfigurational Wavefunctions. *Chemical Physics* **2004,** *304*, 227-236.
29. Gao, J.; Grofe, A.; Ren, H.; Bao, P. Beyond Kohn–Sham Approximation: Hybrid Multistate Wave Function and Density Functional Theory. *J. Phys. Chem. Lett.* **2016,** *7*, 5143-5149.
30. Grofe, A.; Qu, Z.; Truhlar, D. G.; Li, H.; Gao, J. Diabatic-at-Construction (Dac) Method for Diabatic and Adiabatic Ground and Excited States Based on Multistate Density Functional Theory. *J. Chem. Theory Comput.* **2017,** *13*, 1176-1187.
31. Lu, Y.; Gao, J. Multistate Density Functional Theory of Excited States. *J. Phys. Chem. Lett.* **2022**, 7762-7769.
32. Mo, Y.; Bao, P.; Gao, J. Energy Decomposition Analysis Based on a Block-Localized Wavefunction and Multistate Density Functional Theory. *Phys. Chem. Chem. Phys.* **2011,** *13*, 6760-6775.

33. Yu, Q.; Hammes-Schiffer, S. Nuclear-Electronic Orbital Multistate Density Functional Theory. *J. Phys. Chem. Lett.* **2020,** *11*, 10106-10113.
34. Skone, J. H.; Pak, M. V.; Hammes-Schiffer, S. Nuclear-Electronic Orbital Nonorthogonal Configuration Interaction Approach. *J. Chem. Phys.* **2005,** *123*, 134108.
35. Thom, A. J. W.; Head-Gordon, M. Hartree–Fock Solutions as a Quasidiabatic Basis for Nonorthogonal Configuration Interaction. *J. Chem. Phys.* **2009,** *131*, 124113.
36. Lischka, H.; Nachtigallová, D.; Aquino, A. J. A.; Szalay, P. G.; Plasser, F.; Machado, F. B. C.; Barbatti, M. Multireference Approaches for Excited States of Molecules. *Chem. Rev.* **2018,** *118*, 7293-7361.
37. Ghosh, S.; Verma, P.; Cramer, C. J.; Gagliardi, L.; Truhlar, D. G. Combining Wave Function Methods with Density Functional Theory for Excited States. *Chem. Rev.* **2018,** *118*, 7249-7292.
38. Yu, Q.; Schneider, P. E.; Hammes-Schiffer, S. Analytical Gradients for Nuclear–Electronic Orbital Multistate Density Functional Theory: Geometry Optimizations and Reaction Paths. *J. Chem. Phys.* **2022,** *156*, 114115.
39. Hammes-Schiffer, S.; Tully, J. C. Proton Transfer in Solution: Molecular Dynamics with Quantum Transitions. *J. Chem. Phys.* **1994,** *101*, 4657-4667.
40. Crespo-Otero, R.; Barbatti, M. Recent Advances and Perspectives on Nonadiabatic Mixed Quantum–Classical Dynamics. *Chem. Rev.* **2018,** *118*, 7026-7068.
41. Curchod, B. F. E.; Martínez, T. J. Ab Initio Nonadiabatic Quantum Molecular Dynamics. *Chem. Rev.* **2018,** *118*, 3305-3336.
42. Li, X.; Tully, J. C.; Schlegel, H. B.; Frisch, M. J. Ab Initio Ehrenfest Dynamics. *J. Chem. Phys.* **2005,** *123*, 084106.
43. Tully, J. C. Molecular Dynamics with Electronic Transitions. *J. Chem. Phys.* **1990,** *93*, 1061-1071.
44. Tully, J. C. Mixed Quantum-Classical Dynamics. *Faraday Discussions* **1998,** *110*, 1-13.
45. Coutinho-Neto, M. D.; Viel, A.; Manthe, U. The Ground State Tunneling Splitting of Malonaldehyde: Accurate Full Dimensional Quantum Dynamics Calculations. *J. Chem. Phys.* **2004,** *121*, 9207-9210.
46. Hazra, A.; Skone, J. H.; Hammes-Schiffer, S. Combining the Nuclear-Electronic Orbital Approach with Vibronic Coupling Theory: Calculation of the Tunneling Splitting for Malonaldehyde. *J. Chem. Phys.* **2009,** *130*, 054108.
47. Käser, S.; Unke, O. T.; Meuwly, M. Reactive Dynamics and Spectroscopy of Hydrogen Transfer from Neural Network-Based Reactive Potential Energy Surfaces. *New Journal of Physics* **2020,** *22*, 055002.
48. Meek, G. A.; Levine, B. G. Evaluation of the Time-Derivative Coupling for Accurate Electronic State Transition Probabilities from Numerical Simulations. *J. Phys. Chem. Lett.* **2014,** *5*, 2351-2356.
49. Tully, J. C. Perspective: Nonadiabatic Dynamics Theory. *J. Chem. Phys.* **2012,** *137*, 22A301.
50. Epifanovsky, E.; Gilbert, A. T. B.; Feng, X.; Lee, J.; Mao, Y.; Mardirossian, N.; Pokhilko, P.; White, A. F.; Coons, M. P.; Dempwolff, A. L.; Gan, Z.; Hait, D.; Horn, P. R.; Jacobson, L. D.; Kaliman, I.; Kussmann, J.; Lange, A. W.; Lao, K. U.; Levine, D. S.; Liu, J.; McKenzie, S. C.; Morrison, A. F.; Nanda, K. D.; Plasser, F.; Rehn, D. R.; Vidal, M. L.; You, Z.-Q.; Zhu, Y.; Alam, B.; Albrecht, B. J.; Aldossary, A.; Alguire, E.; Andersen, J. H.; Athavale, V.; Barton, D.; Begam, K.; Behn, A.; Bellonzi, N.; Bernard, Y. A.; Berquist, E. J.; Burton, H. G. A.; Carreras, A.; Carter-

Fenk, K.; Chakraborty, R.; Chien, A. D.; Closser, K. D.; Cofer-Shabica, V.; Dasgupta, S.; de Wergifosse, M.; Deng, J.; Diedenhofen, M.; Do, H.; Ehlert, S.; Fang, P.-T.; Fatehi, S.; Feng, Q.; Friedhoff, T.; Gayvert, J.; Ge, Q.; Gidofalvi, G.; Goldey, M.; Gomes, J.; González-Espinoza, C. E.; Gulania, S.; Gunina, A. O.; Hanson-Heine, M. W. D.; Harbach, P. H. P.; Hauser, A.; Herbst, M. F.; Hernández Vera, M.; Hodecker, M.; Holden, Z. C.; Houck, S.; Huang, X.; Hui, K.; Huynh, B. C.; Ivanov, M.; Jász, Á.; Ji, H.; Jiang, H.; Kaduk, B.; Kähler, S.; Khistyaev, K.; Kim, J.; Kis, G.; Klunzinger, P.; Koczor-Benda, Z.; Koh, J. H.; Kosenkov, D.; Koulias, L.; Kowalczyk, T.; Krauter, C. M.; Kue, K.; Kunitsa, A.; Kus, T.; Ladjánszki, I.; Landau, A.; Lawler, K. V.; Lefrancois, D.; Lehtola, S.; Li, R. R.; Li, Y.-P.; Liang, J.; Liebenthal, M.; Lin, H.-H.; Lin, Y.-S.; Liu, F.; Liu, K.-Y.; Loipersberger, M.; Luenser, A.; Manjanath, A.; Manohar, P.; Mansoor, E.; Manzer, S. F.; Mao, S.-P.; Marenich, A. V.; Markovich, T.; Mason, S.; Maurer, S. A.; McLaughlin, P. F.; Menger, M. F. S. J.; Mewes, J.-M.; Mewes, S. A.; Morgante, P.; Mullinax, J. W.; Oosterbaan, K. J.; Paran, G.; Paul, A. C.; Paul, S. K.; Pavošević, F.; Pei, Z.; Prager, S.; Proynov, E. I.; Rák, Á.; Ramos-Cordoba, E.; Rana, B.; Rask, A. E.; Rettig, A.; Richard, R. M.; Rob, F.; Rossomme, E.; Scheele, T.; Scheurer, M.; Schneider, M.; Sergueev, N.; Sharada, S. M.; Skomorowski, W.; Small, D. W.; Stein, C. J.; Su, Y.-C.; Sundstrom, E. J.; Tao, Z.; Thirman, J.; Tornai, G. J.; Tsuchimochi, T.; Tubman, N. M.; Veccham, S. P.; Vydrov, O.; Wenzel, J.; Witte, J.; Yamada, A.; Yao, K.; Yeganeh, S.; Yost, S. R.; Zech, A.; Zhang, I. Y.; Zhang, X.; Zhang, Y.; Zuev, D.; Aspuru-Guzik, A.; Bell, A. T.; Besley, N. A.; Bravaya, K. B.; Brooks, B. R.; Casanova, D.; Chai, J.-D.; Coriani, S.; Cramer, C. J.; Cserey, G.; DePrince, A. E.; DiStasio, R. A.; Dreuw, A.; Dunietz, B. D.; Furlani, T. R.; Goddard, W. A.; Hammes-Schiffer, S.; Head-Gordon, T.; Hehre, W. J.; Hsu, C.-P.; Jagau, T.-C.; Jung, Y.; Klamt, A.; Kong, J.; Lambrecht, D. S.; Liang, W.; Mayhall, N. J.; McCurdy, C. W.; Neaton, J. B.; Ochsenfeld, C.; Parkhill, J. A.; Peverati, R.; Rassolov, V. A.; Shao, Y.; Slipchenko, L. V.; Stauch, T.; Steele, R. P.; Subotnik, J. E.; Thom, A. J. W.; Tkatchenko, A.; Truhlar, D. G.; Van Voorhis, T.; Wesolowski, T. A.; Whaley, K. B.; Woodcock, H. L.; Zimmerman, P. M.; Faraji, S.; Gill, P. M. W.; Head-Gordon, M.; Herbert, J. M.; Krylov, A. I. Software for the Frontiers of Quantum Chemistry: An Overview of Developments in the Q-Chem 5 Package. *J. Chem. Phys.* **2021,** *155*, 084801.

51. Lee, C.; Yang, W.; Parr, R. G. Development of the Colle-Salvetti Correlation-Energy Formula into a Functional of the Electron Density. *Phys. Rev. B* **1988,** *37*, 785.

52. Becke, A. D. Density-Functional Thermochemistry. Iii. The Role of Exact Exchange. *J. Chem. Phys.* **1993,** *98*, 5648-5652.

53. Dunning, T. H., Jr. Gaussian Basis Sets for Use in Correlated Molecular Calculations: 1. The Atoms Boron through Neon and Hydrogen. *J. Chem. Phys.* **1989,** *90*, 1007-1023.

54. Yu, Q.; Pavošević, F.; Hammes-Schiffer, S. Development of Nuclear Basis Sets for Multicomponent Quantum Chemistry Methods. *J. Chem. Phys.* **2020,** *152*, 244123.

55. Culpitt, T.; Yang, Y.; Pavošević, F.; Tao, Z.; Hammes-Schiffer, S. Enhancing the Applicability of Multicomponent Time-Dependent Density Functional Theory. *J. Chem. Phys.* **2019,** *150*, 201101.

For Table of Contents Only